Closer to Photosystem II: A Co$_4$O$_4$ Cubane Catalyst with Flexible Ligand Architecture

Fabio Evangelisti, Robin Güttinger, René Moré, Sandra Luber, and Greta R. Patzke*

Department of Chemistry, University of Zurich, Winterthurerstrasse 190, CH-8057 Zurich, Switzerland

S *Supporting Information*

ABSTRACT: We introduce the novel Co$_4$O$_4$ complex [Co$^{II}_4$(hmp)$_4$(μ-OAc)$_2$(μ_2-OAc)$_2$(H$_2$O)$_2$] (**1**) (hmp = 2-(hydroxymethyl)pyridine) as the first Co(II)-based cubane water oxidation catalyst. Monodentate acetate and aqua ligands lend the flexible environment of **1** closest resemblance to photosystem II among its tetranuclear mimics to date. Visible-light-driven catalytic activity of **1** increases with pH value through aqua ligand deprotonation. The Co(II) core combines robustness and stability with flexibility through a new type of water-oxidation mechanism via mobile ligands.

Artificial photosynthesis as the most visionary and challenging solution for tomorrow's energy problems[1,2] depends on the development of efficient visible-light-driven water oxidation catalysts (WOCs) to widen this bottleneck toward water splitting.[3,4] Nature's cuboidal CaMn$_4$O$_5$ oxygen evolving complex (OEC) of photosystem II (PSII) is the key paradigm for biomimetic WOC design.[5−7] To date, however, the synthesis of high performance Mn-cubane water oxidation catalysts still remains challenging,[8−11] and the number of known Co$_4$O$_4$-based WOCs is limited to selected Co(III)-containing representatives so far.[12−15]

Here, we pave new ways to PSII mimics with the first Co(II)-based cubane WOC: the novel complex [Co$^{II}_4$(hmp)$_4$(μ-OAc)$_2$(μ_2-OAc)$_2$(H$_2$O)$_2$] (**1**) (hmp = 2-(hydroxymethyl)pyridine) approaches OEC pathways through a ligand environment of unprecedented flexibility.

Whereas cuboidal Co motifs have recently been successfully implemented in heterogeneous WOCs, such as cobalt-phosphate (Co-Pi)[16] or spinel-type catalysts,[17] the quest for homogeneous multinuclear Co-based WOCs remains a complex forefront task with only few selection guidelines at hand.[18,19] This is, for example, evident from the few cobalt-containing polyoxometalate WOCs, such as [Co$_4$(H$_2$O)$_2$(PW$_9$O$_{34}$)$_2$]$^{10−}$,[20] which have been identified among this rapidly growing compound family[21] over the past years.[22] Likewise, after decades of studies on the structural and single molecule magnet (SMM) properties of Co$_4$O$_4$ cubanes,[23] only [Co$^{III}_4$O$_4$(OAc)$_4$(py)$_4$] and the corresponding [Co$^{III}_4$O$_4$(OAc)$_4$(p-NC$_5$H$_4$X)$_4$] (X = H, Me, t-Bu, OMe, Br, OAc, CN) series were recently implemented as high performance WOCs.[12−14] [Co$^{III}_4$O$_4$(OAc)$_2$(bpy)$_4$](ClO$_4$)$_2$ and [Co$^{III}_4$O$_4$(CO$_2$Py)$_2$(bpy)$_4$](ClO$_4$)$_2$ (CO$_2$Py = 4-carboxypyridine) linked to Re^I photosensitizers were furthermore studied as model systems.[15,24] The Co(III) centers in these cubanes are mainly stabilized through rigid bidentate ligands, in contrast to

the flexible PSII-OEC with its manifold water exchange steps on the way to oxygen release.[5,25] Considerably less is known about the pathways of Co-cubane WOCs, and the only modeling studies to date have been performed for {Co$^{III}_4$O$_4$(H$_2$O)$_{12}$} as a hypothetical compound[26,27] along with [Co$^{III}_4$O$_4$-(OAc)$_4$(py)$_4$].[27]

The current need for operational Co-cubane catalysts with nature's structural versatility has inspired us to newly create WOC **1** featuring a uniquely open ligand environment (Figure 1). Cubane **1** bears closest resemblance to the PSII-OEC
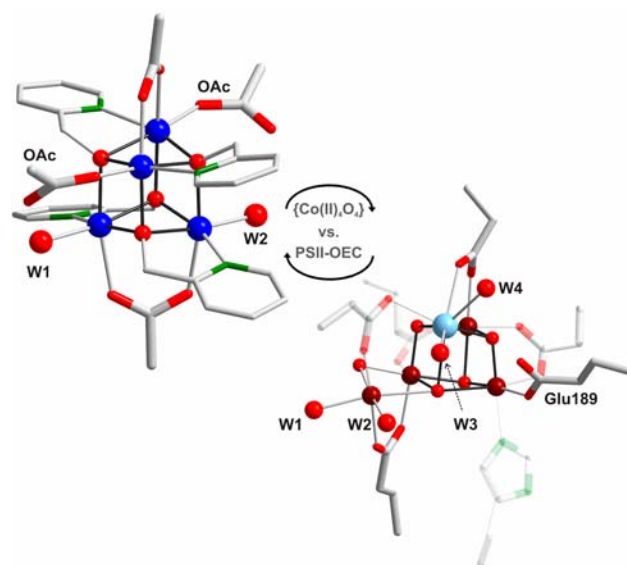
Figure 1. Crystal structure of [Co$^{II}_4$(hmp)$_4$(μ-OAc)$_2$(μ_2-OAc)$_2$-(H$_2$O)$_2$] (hmp = 2-(hydroxymethyl)pyridine) (**1**) (left: Co, dark blue; O, red; N, green; C, gray; H atoms were omitted for clarity) vs PSII-OEC (right: Mn, brown; Ca, light blue).[28]

hitherto through progress in core and shell design: (1) Co(II) centers are first introduced into a cubane WOC. (2) Here, they are equipped with flexible aqua ligands, giving rise to enhanced WOC performance through deprotonation and ligand exchange. (3) Two monodentate acetate ligands are attached to the substitutionally labile Co(II) core atoms. (4) This provides a new experimental basis for modeling PSII-inspired water oxidation mechanisms.

In the following, we illustrate how the title compound tackles key challenges of current WOC development through structural innovation, biorelated pathways, enhanced catalyst stability, and novel input for computational studies.

Characterization of 1. Compound **1** was obtained from the reaction of $Co(OAc)_2 \cdot 4H_2O$ and 2-(hydroxymethyl)pyridine under reflux conditions as described in the Supporting Information. The solid-state structure of **1** was established from single crystal X-ray diffraction data (for crystallographic details and further analyses, cf. the Supporting Information). The hmp ligands stabilize the cubane motif of **1**, which is in line with the recently reported $Ni(II)_4O_4$ analogue.[29] The phase purity was confirmed with powder X-ray diffraction, thermogravimetric analyses, and Fourier-transform infrared (FT-IR) spectra (Figures S2−S4). All Co(II) centers are coordinated in a slightly distorted octahedral geometry consisting of one nitrogen atom of the bidentate hmp ligands, three μ_3-oxygen atoms, and a fourth oxygen atom of the bridging acetate ligands. The fifth oxygen atom is contributed by the monodentate ligands located on opposite cluster planes, namely, H_2O (bottom: Co(1) and Co(2)) and acetate (top: Co(3) and Co(4); cf. Figure 1). The presence of the $[Co^{II}_4(hmp)_4]^{4+}$ core of **1** in solution was established with high resolution electrospray-ionization mass spectrometry (HR-ESI-MS). The main ion peak of **1** in methanol at m/z 844.95327 $[C_{30}H_{33}Co_4N_4O_{10}^+; -1.60$ ppm] can be assigned to the $[Co^{II}_4(hmp)_4(OAc)_3]^+$ fragment which is formed through loss of one monodentate acetate and two aqua ligands (Figure S5). Further ion peaks at m/z 767.92631 $[C_{25}H_{30}Co_4N_3O_{10}^+; -1.22$ ppm] and m/z 690.89963 $[C_{20}H_{27}Co_4N_2O_{10}^+; -1.17$ ppm] arise from the replacement of hmp ligands by methanolate, affording the $[Co^{II}_4(hmp)_3(OAc)_3(OMe)]^+$ and $[Co^{II}_4(hmp)_2(OAc)_3(OMe)_2]^+$ fragments, respectively. Given that the oxygen evolution performance of **1** strongly increases with pH value (cf. section below), the pK_a value for deprotonation of both aqua ligands in rapid succession was determined as 8.7 from spectrophotometric titrations together with a second pK_a value around 5.8, indicating the titration of dissociated monodentate acetate groups (Figure S7). As Co cubanes with aqua ligands have proven quite elusive, their dissociation and exchange processes remain to be explored. Interestingly, the pK_a value for **1** is well in line with the first water exchange studies on Co(II) heteropolyoxotungstates which revealed pK_a values around 8 for their core aqua ligands.[30] The aqua ligands of **1** thus remain intact in neutral media, followed by an increasing degree of deprotonation under alkaline catalytic conditions (pH 8−9 in borate buffer). This clearly differentiates **1** from the previously reported Co(III)-containing cubanes, where the absence of aqua ligands renders the bridging μ_3-O in the Co_4O_4 core the primary target for (de)protonation steps.[12,14]

FT-IR spectra of **1** before and after exchange experiments with CD_3COOD display a shift of the CD_3 deformation mode (Figure S8). X-ray absorption spectra of cobalt cubanes in solution remain rather unexplored to the best of our knowledge. We newly confirmed the solution stability of **1** with X-ray absorption near edge structure (XANES) and extended X-ray absorption fine structure (EXAFS) spectra recorded on solid samples and in buffered solutions. EXAFS data could be fitted with structural models on the basis of the single crystal structure (Figures S9 and S10, Table S4). Fits of solution EXAFS spectra only point to minor structural changes, which arise from contraction of Co−O and of Co−N bond lengths as well as of Co···Co distances, which does not disagree with the postulated ligand dissociation and exchange (Figures S10 and S11).

Catalytic Performance. Photocatalytic water oxidation activity of **1** in the presence of $[Ru(bpy)_3]^{2+}$ as photosensitizer (PS) and $S_2O_8^{2-}$ as sacrificial electron acceptor was monitored with complementary techniques, i.e., via gas chromatography and with Clark electrodes in solution (Figures S12 and S15).[31] pH-dependent WOC performance of **1** was evaluated under standard conditions (cf. Figure 2 and the Supporting Information for
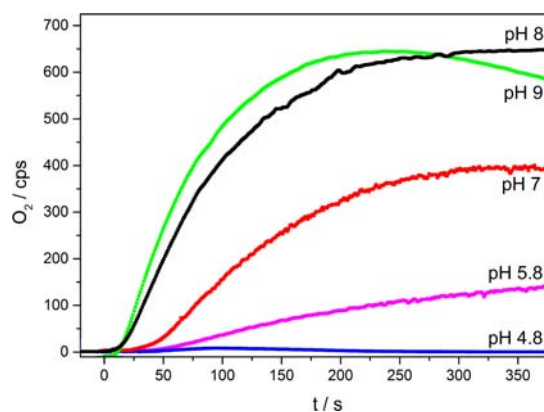
Figure 2. Visible-light-driven WOC activity of **1** (Clark electrode monitoring, 1 mM $[Ru(bpy)_3]^{2+}$, 5 mM $Na_2S_2O_8$, 470 nm) for different catalyst concentrations (cf. Table 1) and buffer systems at pH 4.8, pH 5.8, pH 7, pH 8, and pH 9.

experimental details) over a pH range from 4.8 to 9 in different buffers with maximum O_2 yield for a pH value of 8 and the highest turnover frequency (TOF) at pH 9.

The dependence of O_2-evolution kinetics on the WOC concentration changes notably over the pH range from 7 to 9 (cf. Figures S14−S16). Whereas the rate laws at pH 7 and 8 are not straightforward over the investigated WOC concentration range $(40−200\ \mu M)$, the kinetics at pH 9 clearly change toward a linear trend below 60 μM of **1** (Figure S17). Concentration- and pH-dependent WOC performance of **1** (Figure 3) is summarized for optimized catalyst concentrations in Table 1 (highest TOFs only;[32] for complete data, cf. Table S6). TOF increases with the pH value from 1.8 s^{-1} (pH 7) to 7.0 s^{-1} (pH 9). The productive influence of higher pH values on the catalytic activity of **1** is furthermore illustrated by a turnover number (TON) increase from 20 (pH 7) to 35 (pH 8), and a maximum TON value of 40 is
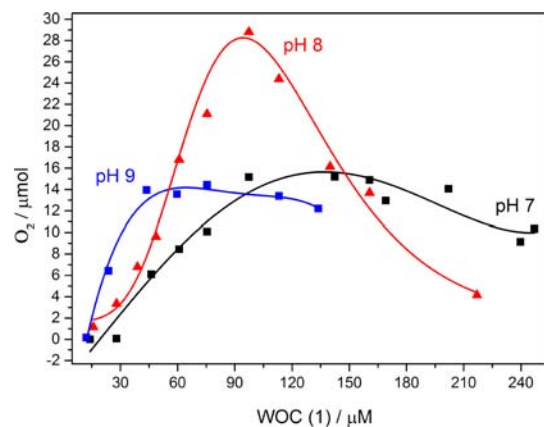
Figure 3. Concentration-dependent photochemical O_2 evolution for **1** under standard conditions (1 mM $[Ru(bpy)_3]^{2+}$, 5 mM $Na_2S_2O_8$, 470 nm) at pH 7 (black), pH 8 (red), and pH 9 (blue).

18735

dx.doi.org/10.1021/ja4098302 | J. Am. Chem. Soc. 2013, 135, 18734−18737

Table 1. WOC Performance of 1 as a Function of pH Value and Optimized Catalyst Concentration

pH^a	WOC^b (μM)	$yield^c$ (%)	TOF^d (s^{-1})	TON
7	98	75	1.8	20
8	60	83	4.4	35
9	60	69	7.0	28

[a]Buffer media (cf. also Figure 2): pH 4.8 (40 mM NaOAc/HOAc), pH 5.8 (30 mM Na_2SiF_6/NaHCO$_3$), pH 7 (40 mM Na_2HPO_4/NaH$_2$PO$_4$), pH 8 and 9 (50 mM borate adjusted with HCl). [b]Concentration range investigated for **1**: 10−250 μM (cf. Table S6 for complete data range). [c]Based on maximum theoretical O_2 yields corresponding to 50% of initial $Na_2S_2O_8$ quantities. [d]Initial linear slope of O_2 concentration divided by time and catalyst concentration (cf. the Supporting Information for experimental details).

observed for lower WOC concentrations (43 μM) at pH 9 (Table S6). This trend indicates that deprotonation of the aqua ligands of **1** accelerates the water oxidation process.

Catalyst Stability. Recently, the challenging interplay of homogeneous and heterogeneous WOCs[33,34] has gained new momentum with respect to Co-containing polyoxometalate catalysts.[19] We thus investigated the promising potential of Co-cubane WOCs to circumvent the stability issues which remain in the way of homogeneous Mn-based PSII analogues after decades of intense research.[4,9]

CV of pristine **1** in the pH 7−9 range (Figure S18; pristine **1** vs Co^{2+} and [Ru(bpy)$_3$]$^{2+}$ cf. Figure S20) and of **1** before and after water oxidation confirms the reversibility of the Co^{2+}/Co^{3+} redox couple at 0.5 V (cf. Figures S21 and S22, for representative data at pH 9 and for pH-dependent data and various scan rates in buffer media, respectively). The electrochemical behavior of **1** differs from previously reported Co(III)-cubane WOCs which operate via [$3Co^{III}$−Co^{IV}] redox couples.[12,14,15] The redox potential of the single electron transfer process $1 \rightarrow 1^+$ is constant over the pH range 2.5−8 (cf. the Pourbaix diagram in Figure S19), followed by a linear decrease between pH 8 and 11 (0.1 V/pH unit). The pK_a value of 8.7 for **1** corresponds well to the intersection of both curve branches. As the optimum pH range for WOC tests coincides with the onset of the observed potential decrease, the data trend toward a double proton-coupled electron transfer mechanism with release of two protons per electron is currently further investigated. The stability of **1** under operational conditions was confirmed by comparison of CV data to reference data of unstable Co^{2+}-based WOCs (Figures S20 and S21).

Moreover, UV/vis (Figure S6) and FT-IR spectra (Figures S8 and S27) provide strong evidence that **1** enters the photocatalytic cycle structurally intact. Additionally, representative reaction mixtures were subjected to dynamic light scattering (DLS) analyses after the catalytic cycle to check for nanoparticles (NPs)

above 1 nm in size. DLS of **1** in catalytic media did not display any NP formation after 60 min of visible light irradiation (data not shown), whereas $Co(OAc)_2 \cdot 6H_2O$ formed two particle fractions under analogous conditions (NPs and larger clusters, cf. Figure S23). Operational stability of **1** vs Co^{2+} is even more evident from visual inspection of catalytic vials (Figure S24) and from kinetic comparisons between water oxidation with Co^{2+}-based WOCs and **1**, respectively, over the concentration range from 100 nm to 1 μM (Figure S25). The Co^{2+}-based catalyst exhibits an increasing delay in the onset of O_2 evolution toward higher concentrations (25−27 s),[12] which is characteristic for the conversion of Co^{2+} precatalysts into active CoO_x NPs. This effect is absent for **1**; i.e., no particles are formed in line with DLS results (Figures S23 and S24). Recycling of **1** after addition of fresh $Na_2S_2O_8$ and readjustment of the pH value afforded up to 80% of the original catalytic activity for **1**. A more pronounced decline of O_2 evolution after the third cycle is likely due to PS decomposition (cf. Figure S26 and Table S7 vs Figure S10).

New Perspectives for PSII Analogues. Despite major progress in the synthesis of tetranuclear Mn clusters, they have been found to generate active oxide phases as true catalysts.[4] Although PSII still outperforms its Co mimic **1** by far, the new WOC compares well to leading polynuclear transition metal WOCs in terms of TON (Table 2).

The stable Co(II) cubane **1** combines three biomimetic principles. First, the presence of monodentate and bidentate acetate ligands lends **1** both flexibility and a stable core. Note that PSII-OEC in the recently published X-ray structure with a resolution of 1.9 Å is surrounded by five bridging and one monodentate (Glu189) carboxylate residue as well (Figure 1).[28] Next, the first implementation of aqua ligands in a synthetic cubane WOC is a major step toward O−O formation pathways via water attack and exchange processes which are inspired by the proposed PSII-OEC mechanisms, namely, either nucleophilic attack of Ca^{2+}-bound water on a μ-oxo bridge or its oxo/oxyl-radical coupling with a neighboring water molecule.[5] Third, the $Co(II)_4O_4$ core is superior to Co(III)-based cubanes with respect to substitution lability as an essential prerequisite for homogeneous WOCs.[38]

Employing a high-spin state for Co(II), a remarkably high accordance is found between the $Co(II)_4O_4$ core obtained from the X-ray structure and from geometry optimizations using density-functional theory (this applies especially to the $S = 6$ state (cf. Table S8)). Calculations using a low-spin state for each Co(II) atom lead most notably to a significantly smaller Co(1)−Co(2) distance. Furthermore, the $S = 6$ ground state has been observed for the structurally related SMM [Co^{II}_4(hmp)$_4$-(MeOH)$_4$Cl$_4$].[39] These findings, in combination with the above-mentioned EXAFS stability investigations in solution vs solid phase, suggest the presence of high-spin Co(II) centers in **1**,

Table 2. Key Parameters of 1 Compared to Reference WOCs

WOC type and conditions	TON	TOF^a (s^{-1})	ref
[Co^{II}_4(hmp)$_4$(μ-OAc)$_2$(μ_2-OAc)$_2$(H$_2$O)$_2$]^b	40	7	this work
[$Co^{III}_4O_4$(OAc)$_4$(py)$_4$]^b	40	2×10^{-2}	12
[$Co^{III}_4O_4$(OAc)$_4$(p-C$_5$H$_4$X)$_4$]^b	140	7×10^{-2}	13
[Co_4(H$_2$O)$_2$(PW$_9$O$_{34}$)$_2$]$^{10-}$ ^{b}	75	5	20
[{Ru$_4$O$_4$(OH)$_2$(H$_2$O)$_4$}(γ-SiW$_{10}$O$_{36}$)$_2$]$^{10-}$ ^{c}	500	1.25×10^{-1}	35
[{Ru$_3$O$_3$(H$_2$O)Cl$_2$}(SiW$_9$O$_{34}$)]$^{7-}$ ^{b}	23	7×10^{-1}	36
PSII^d	5×10^2	10^7	37

[a]TOFs were determined by different methods and are thus not further compared. [b][Ru^{III}(bpy)$_3$]$^{2+}$/S$_2$O$_8$$^{2-}$. [c]Ce^{IV}. [d]Tyrosine radical.

which is expected to favor a radical-coupling mechanism compared to low-spin Co(III)/Co(IV) centers.[27] This relates **1** closer to the suggested mechanisms for the high-spin Mn centers in PSII-OEC than the reported Co(III)-cubane WOC prototype.[5,12−14,27]

All in all, $[Co^{II}_4(hmp)_4(\mu\text{-OAc})_2(\mu_2\text{-OAc})_2(H_2O)_2]$ (**1**) is the first Co-cubane WOC working via Co(II) centers, and it promotes WOC development on several levels: An unprecedentedly flexible architecture of monodentate acetate and aqua ligands renders it the closest operational PSII-OEC mimic among the highly sought after cubane WOCs to date. Furthermore, **1** combines active ligand deprotonation and exchange processes with high solution stability, in line with the motto "reactive shell and stable core". Finally, the unique $Co^{II}_4O_4$ WOC provides innovative biomimetic input for new mechanistic modeling to translate the water oxidation pathways of PSII into straightforward catalytic concepts. Quantum chemical calculations are in progress, and they support the expectation that the novel Co(II)-cubane features high-spin Co(II) centers (cf. Table S8), so that explorations of OEC-related mechanisms and investigations for SMM behavior are under way. In summary, we introduce a new Co(II)-cubane water oxidation catalyst prototype which paves the way to tunable PSII mimics.

■ ASSOCIATED CONTENT

Ⓢ Supporting Information

Synthetic protocols, crystallographic data and analytical/electrochemical characterization of **1**, experimental details for photocatalytic investigations, kinetic analyses, stability tests, and quantum chemical calculations. Atomic coordinates have been deposited in the Cambridge Structural Database, Cambridge Crystallographic Data Centre, http://www.ccdc.cam.ac.uk, CCDC 953633. This material is available free of charge via the Internet at http://pubs.acs.org.

■ AUTHOR INFORMATION

Corresponding Author
greta.patzke@aci.uzh.ch

Notes
The authors declare no competing financial interest.

■ ACKNOWLEDGMENTS

■ REFERENCES

(1) McConnell, I.; Li, G. H.; Brudvig, G. W. *Chem. Biol.* **2010**, *17*, 434.
(2) Lewis, N. S.; Nocera, D. G. *Proc. Natl. Acad. Sci. U.S.A.* **2006**, *43*, 15729.
(3) Young, K. J.; Martini, L. A.; Milot, R. L.; Snoeberger, R. C.; Batista, V. S.; Schmuttenmaer, C. A.; Crabtree, R. H.; Brudvig, G. W. *Coord. Chem. Rev.* **2012**, *256*, 2503.
(4) Singh, A.; Spiccia, L. *Coord. Chem. Rev.* **2013**, *257*, 2607.
(5) Cox, N.; Pantazis, D. A.; Neese, F.; Lubitz, W. *Acc. Chem. Res.* **2013**, *46*, 1588.
(6) Dau, H.; Limberg, C.; Reier, T.; Risch, M.; Roggan, S.; Strasser, P. *ChemCatChem* **2010**, *2*, 724.
(7) Luber, S.; Rivalta, I.; Umena, Y.; Kawakami, K.; Shen, J.-R.; Kamiya, N.; Brudvig, G. W.; Batista, V. S. *Biochemistry* **2011**, *50*, 6308.
(8) Brimblecombe, R.; Koo, A.; Dismukes, G. C.; Swiegers, G. F.; Spiccia, L. *J. Am. Chem. Soc.* **2010**, *132*, 2892.
(9) Sun, L.; Hammarström, L.; Åkermark, B.; Styring, S. *Chem. Soc. Rev.* **2001**, *30*, 36.
(10) Tsui, E. Y.; Agapie, T. *Proc. Natl. Acad. Sci. U.S.A.* **2013**, *110*, 10084.
(11) Wiechen, M.; Berends, H. M.; Kurz, P. *Dalton Trans.* **2012**, *41*, 21.
(12) McCool, N. S.; Robinson, D. M.; Sheats, J. E.; Dismukes, G. C. *J. Am. Chem. Soc.* **2011**, *133*, 11446.
(13) Berardi, S.; La Ganga, G.; Natali, M.; Bazzan, I.; Puntoriero, F.; Sartorel, A.; Scandola, F.; Campagna, S.; Bonchio, M. *J. Am. Chem. Soc.* **2012**, *134*, 11104.
(14) La Ganga, G.; Puntoriero, F.; Campagna, S.; Bazzan, I.; Berardi, S.; Bonchio, M.; Sartorel, A.; Natali, M.; Scandola, F. *Faraday Discuss.* **2012**, *155*, 177.
(15) Symes, M. D.; Surendranath, Y.; Luttermann, D. A.; Nocera, D. G. *J. Am. Chem. Soc.* **2011**, *133*, 5174.
(16) McAlpin, J. G.; Stich, T. A.; Ohlin, G. A.; Surendranath, Y.; Nocera, D. G.; Casey, W. H.; Britt, R. D. *J. Am. Chem. Soc.* **2011**, *133*, 15444.
(17) Gardner, G. P.; Go, Y. B.; Robinson, D. M.; Smith, P. F.; Hadermann, J.; Abakumov, A.; Greenblatt, M.; Dismukes, G. C. *Angew. Chem., Int. Ed.* **2012**, *51*, 1616.
(18) Artero, V.; Fontecave, M. *Chem. Soc. Rev.* **2013**, *42*, 2338.
(19) (a) Stracke, J. J.; Finke, R. G. *J. Am. Chem. Soc.* **2011**, *133*, 14872. (b) Vickers, J. W.; Lv, H.; Sumliner, J. M.; Zhu, G.; Luo, Z.; Musaev, D. G.; Geletii, Y. V.; Hill, C. L. *J. Am. Chem. Soc.* **2013**, *135*, 14110.
(20) Yin, Q.; Tan, J. M.; Besson, C.; Geletii, Y. V.; Musaev, D. G.; Kuznetsov, A. E.; Luo, Z.; Hardcastle, K. I.; Hill, C. L. *Science* **2010**, *328*, 342.
(21) Hijazi, A.; Kemmegne-Mbouguen, J. C.; Floquet, S.; Marrot, J.; Fize, J.; Artero, V.; David, O.; Magnier, E.; Pégot, B.; Cadot, E. *Dalton Trans.* **2013**, *42*, 4848.
(22) Soriana-López, J.; Goberna-Ferrón, S.; Vigara, L.; Carbó, J. J.; Poblet, J. M.; Galán-Mascarós, J. R. *Inorg. Chem.* **2013**, *52*, 4753.
(23) Dimitrou, K.; Folting, K.; Streib, W. E.; Christou, G. *J. Am. Chem. Soc.* **1993**, *115*, 6432.
(24) Symes, M. D.; Luttermann, D. A.; Teets, T. S.; Anderson, B. L.; Breen, J. J.; Nocera, D. G. *ChemSusChem* **2013**, *6*, 65.
(25) Siegbahn, P. E. M. *J. Am. Chem. Soc.* **2013**, *135*, 9442.
(26) Wang, L.-P.; Van Voorhis, T. *J. Phys. Chem. Lett.* **2011**, *2*, 2200.
(27) Li, X.; Siegbahn, P. E. M. *J. Am. Chem. Soc.* **2013**, *135*, 13804.
(28) Umena, Y.; Kawakami, K.; Shen, J.-R.; Kamiya, N. *Nature* **2011**, *473*, 55.
(29) Efthymiou, C. G.; Papatriantafyllopoulou, C.; Alexopoulou, N. I.; Raptopoulou, C. P.; Boča, R.; Mrozinski, J.; Balkabassis, E. G.; Perlepes, S. P. *Polyhedron* **2009**, *28*, 3373.
(30) Ohlin, C. A.; Harley, S.; McAlpin, J. G.; Hocking, R. K.; Mercado, B. Q.; Johnson, R. L.; Villa, E. M.; Fidler, M. K.; Olmstead, M. M.; Spiccia, L.; Britt, R. D.; Casey, W. H. *Chem.—Eur. J.* **2011**, *17*, 4408.
(31) Evangelisti, F.; Car, P.-E.; Blacque, O.; Patzke, G. R. *Catal. Sci. Technol.* **2013**, *12*, 3117.
(32) Savini, A.; Belanzoni, P.; Bellachioma, G.; Zuccaccia, D.; Macchioni, A. *Green Chem.* **2011**, *13*, 3360.
(33) Crabtree, R. H. *Chem. Rev.* **2012**, *112*, 1536.
(34) Gerken, J. B.; McAlpin, J. G.; Chen, J. Y. C.; Rigsby, M. L.; Casey, W. H.; Britt, R. D.; Stahl, S. S. *J. Am. Chem. Soc.* **2011**, *133*, 14431.
(35) Sartorel, A.; Carraro, M.; Scorrano, G.; Zorzi, R. D.; Geremia, S.; McDaniel, N. D.; Bernhard, S.; Bonchio, M. *J. Am. Chem. Soc.* **2008**, *130*, 5006.
(36) Car, P.-E.; Guttentag, M.; Baldridge, K. K.; Alberto, R.; Patzke, G. R. *Green Chem.* **2012**, *14*, 1680.
(37) Stewart, A. C.; Bendall, D. S. *Biochem. J.* **1980**, *188*, 351.
(38) Lieb, D.; Zahl, A.; Wilson, E. F.; Streb, C.; Nye, L. C.; Meyer, K.; Ivanović-Burmazović, I. *Inorg. Chem.* **2011**, *50*, 9053.
(39) Yang, E.-C.; Hendrickson, D. N.; Wernsdorfer, W.; Nakano, M.; Zakharov, L. N.; Sommer, R.; Rheingold, A. L.; Ledezma-Gairaud, M.; Christou, G. *J. Appl. Phys.* **2002**, *91*, 7382.